Morphological and Phase Stability of Zinc Blende and Amorphous ZnS Nanoparticles

A.S. Barnard, C.A. Feigl and S.P. Russo

Supplementary Information

At standard temperature and pressure (STP) ZnS is stable in the zinc blende (ZB) solid crystalline phase, otherwise known as sphalerite. The ZB phase belongs to space group 216, possessing a dual basis, face-centred cubic structure with Zn occupying the Wyckoff position (0,0,0) and S at (¼,¼,¼) where neither atom possesses any internal degrees of freedom. Both zinc and sulphur atoms are tetrahedrally coordinated and the ZnS dimers are stacked in an ABCABC arrangement. This crystal structure is illustrated in figure 1. A meta-stable wurtzite (WZ) structure also exists at STP and becomes more stable than the ZB phase above 1020˚C. The WZ structure belongs to space group 186 with Zn at (⅓,⅔,0) and S at (⅓,⅔,⅜) where, in this case, both the Zn and S atoms possess an internal degree of freedom along the *z*-axis. The ZnS dimers are stacked in an ABAB arrangement which produces a hexagonal close-packed system with tetrahedral bonding. At high pressures (above ~15 GPa) the rocksalt phase exists and the Cinnabar phase emerges above ~65 GPa. In nanoparticle form a multifarious combination of factors are responsible for determining the thermodynamically preferred phase of ZnS, which can be either ZB or WZ at STP [1-7]. Experimentally determined mechanical properties and other theoretical calculations of this material for the ZnS in the ZB phase can be found in table 2.

To sample a range of (readily available) *ab intio* methods, we have performed DFT calculations using the plane-wave basis set simulation package VASP, with the Perdew-Wang (PW91) [8] and Perdew-Burke-Ernzerhof (PBE) [9] GGA functionals, and the Ceperly-Alder (CA) [10] LDA functional. The Brillouin zone was sampled with an 8 x 8 x 8 Monkhorst–Pack scheme generated *k*-point mesh. A 12x12x12 mesh was also used while testing on the ZB ZnS bulk structure, however we found that a 12x12x12 *k*-point mesh did not produce any significant changes in the energies, so was not used in further tests. In all cases, energy convergence was achieved to within 10^{-4} eV. Plane Augmented Wave (PAW) basis sets were used with all functionals, and an additional Ultrasoft Pseudopotential basis set (USPP) was used with the PW91 functional. For each XC and pseudopotential combination basis sets with increasingly larger plane wave cut-offs were used, thereby providing increasingly larger basis sets. A summary of our overarching methodology is shown in table 1. The notation used to abbreviate the combination of DFT approximation, XC functional, pseudopotential and basis set used in this paper will henceforth be referred to in the manner as described in the final row of table 1 (designated as Notation) with the plane-wave cut-off given at the end of the notation. For example, a DFT result calculated using the Perdew-Burke-Ernzerhof form of the Generalised Gradient Approximation with a PAW basis set of 300 eV cut-off is referred as GGA|PBE|PAW|300.

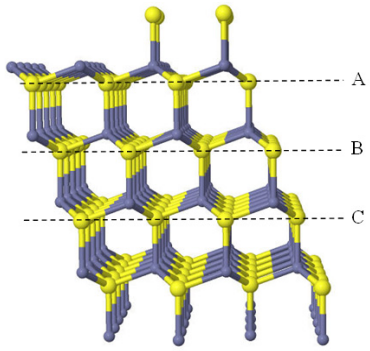

Fig.1 The ZB structure showing the diagonal ABCABC stacking.

Table 1 Summary of methodology and notation convention.

Ab initio Method	DFT			
Density Approximation	LDA	GGA		
XC Functional	CA	PBE	PW91	
Pseudopotential	PAW	PAW	PAW	USPP
Plane-wave Basis set kinetic energy cut-off (eV)	325 400 425 500	325 360 420 470 500	325 360 425 500	275 300 500
Notation	LDA|CA|PAW	GGA|PBEPAW	GGA|PW91|PAW	GGA|PW91|USPP

For simulations of the type described above, the computational cost scales with the size of the basis set, which is determined by the plane-wave cut-off. For this reason it is desirable to use as low a cut-off (small basis set) as possible without reducing the accuracy of the results substantially. In practise, a compromise must be reached between computational cost and accuracy. The choice of kinetic energy cut-off (basis set size) is particularly important when calculating mechanical properties such as elastic constants, because the plane-wave density changes during volumetric dilations.

To test the effect of plane-wave energy cut-off on the accuracy and cost, each structure was fully relaxed (to a convergence of 10^{-4} eV) and then a series of static, single-point energy calculations performed at increasing energy cut-offs. Following the results of these tests, bulk properties in the ZB phase were calculated using plane-wave energy cut-offs of 400, 425 and 500 eV for LDA|CA|PAW; 360, 420, 470 and 500 eV for GGA|PBE|PAW; 360, 425 and 500 eV for

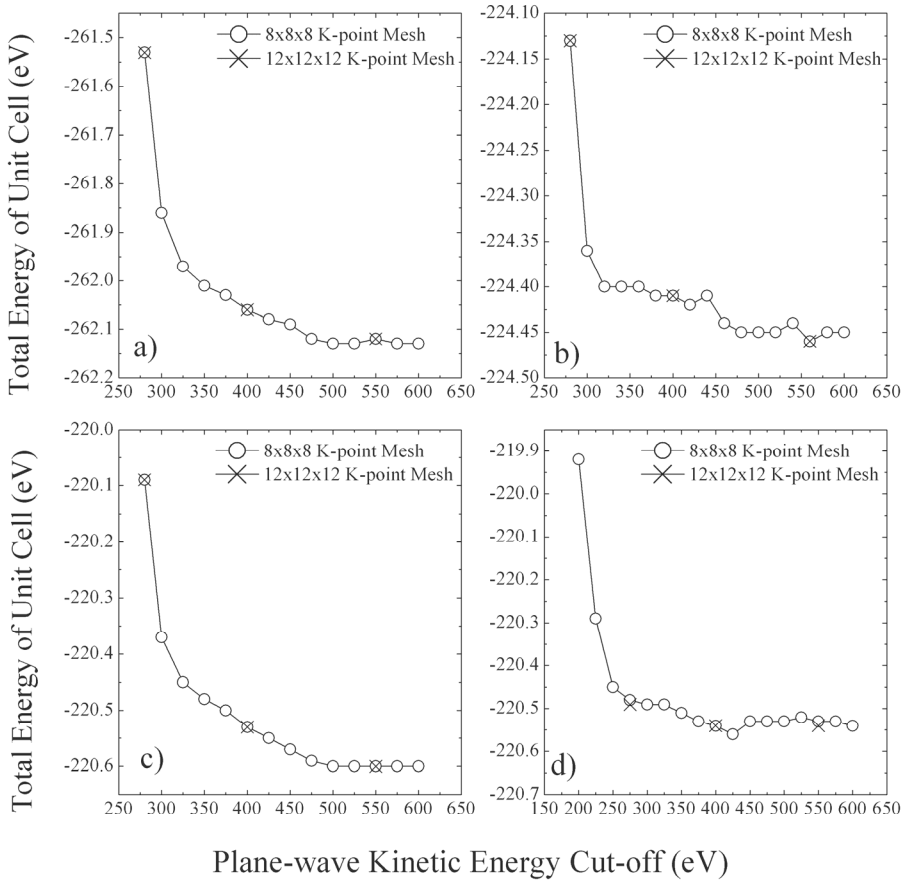

Fig. 2 Total energy as a function of plane-wave energy cut-off for the ZB structure. Calculated using a) LDA|CA|PAW, b) PBE, c) GGA|PW91|PAW and d) GGA|PW91|USPP with 8 x 8 x 8 and 12 x12 x 12 *k*-point mesh sampling. Data lines are for visual guidance only.

GGA|PW91|PAW; and 300 and 500 eV for GGA|PW91|USPP. Bulk properties in the WZ phase were calculated at 325 and 500 eV for all functionals except GGA|PW91|USPP which was tested at 275 and 500 eV, due to the relatively smaller basis set size required to achieve convergence.

The bulk moduli and pressure derivatives of the ZB and WZ were obtained by calculating the total energy for different unit cell volumes and then fitting the data to the third-order Birch-Murnaghan equation of state[11]:

$$E(V) = E_0 + \frac{9}{8}B_0V_0\left[\left(\frac{V_0}{V}\right)^{\frac{2}{3}} - 1\right]^2 + \frac{9}{16}B_0(B_0^{'} - 4)V_0\left[\left(\frac{V_0}{V}\right)^{\frac{2}{3}} - 1\right]^3 \quad (1)$$

where V_o is the unit-cell volume at zero pressure, B_o is the bulk modulus and $B_o^{'}$ is the pressure derivative of the bulk modulus at zero pressure.

For cubic crystals the elastic constants are the second derivatives of the energy density with respect to specific strain components. The C_{11} elastic constant can be determined by applying a small elastic strain in the [100] direction of the lattice (while keeping the lattice fixed in the orthogonal directions). If we represent a strain along the [100] direction by δ and $\partial^2E/\partial\delta^2$ as the second derivative of the total lattice energy with respect to this strain, then the elastic constant C_{11} is given by:

$$C_{11} = \frac{1}{V_o}\cdot\frac{\partial^2 E}{\partial\delta^2} = \frac{2b}{V_o} \quad (2)$$

where V_o is the equilibrium lattice volume and b is the quadratic coefficient in the polynomial fit to an E vs δ curve.

For cubic crystals bulk modulus is related to the elastic constants C_{11} and C_{12} by [12]:

$$B_o = \frac{C_{11} - 2C_{12}}{3} \quad (3)$$

Therefore using equations 2 and 3, the elastic constant C_{12} can also be determined.

In addition to the elastic properties, the enthalpy of formation for the formation of ZnS may be determined using:

$$\Delta H_{ZnS} = E_{ZnS} - (N_{Zn}\mu_{Zn} + N_S\mu_S) \quad (4)$$

where N_i is the number of atoms of element i in the relaxed structure of ZnS and μ_i is the chemical potential of element i. Since only the final stage of the reaction sequence is treated explicitly, it is important to select the μ_i carefully to match the experimental conditions. In this case Zn is included in the bulk form, and S in molecular form. However, since oxygen is not included in the reaction cycle, results for two different S molecules are included for comparison: S_2 and S_8.

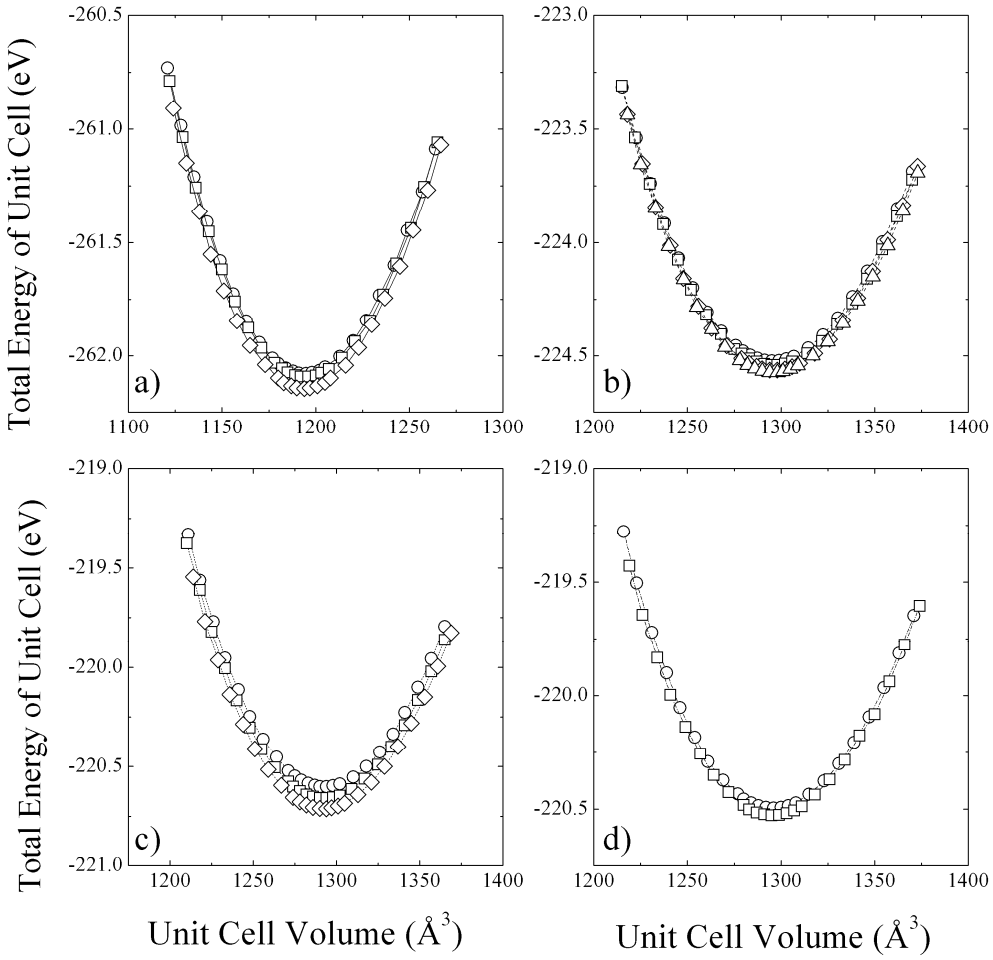

Fig. 3 Total energy as a function of volume for the ZB structure. Calculated using a) LDA|CA|PAW with plane-wave energy cut-offs of 400(○), 425(□) and 500(◊) eV; b) GGA|PBE|PAW at 360(○), 420(□) 470(◊) and 500(**Δ**) eV, c) GGA|PW91|PAW at 360(○) 425(□) and 500(◊) eV and d) GGA|PW91|USPP at 300(○) and 500(□) eV.

Therefore, the chemical potential of zinc was calculated in the hexagonal phase in the following manner:

$$\mu_{Zn} = \frac{1}{N} E_{Zn}^{hex} \quad (5)$$

where E_{Zn}^{hex} is the DFT energy of bulk Zn metal (which has an hexagonal structure $P6_3/mmc$, space group 194) and N is the number of zinc atoms in the hexagonal zinc structure.

The chemical potential of sulphur was calculated using the S_8 and S_2 molecules, using equations 6 and 7:

$$\mu_S(S_8) = \frac{1}{8} E_{S8} \quad (6)$$

$$\mu_S(S_2) = \frac{1}{2} E_{S2} \quad (7)$$

where E_{S8} and E_{S2} are the zero-point DFT energies of the S_8 and S_2 molecules respectively.

Figure 2 gives shows the variation in total energy of a geometry optimised ZB structure as a function of plane-wave cut-off. In all cases the variation in total energy with cut-off for values about 500 eV is very small indicating the 500 eV is the best plane wave cut-off value for calculating elastic moduli, which require energies to be calculated over small volume changes. However for particular combinations of functional and basis-set there exist small plateau regions in the energy-plane wave cut-off curve at lower cut-off values, for example at 350eV using GGA|PBE|PAW and 300 eV using GGA|PW91|USPP, therefore these values of plane-wave cut-off could possibly also be used with a reasonable saving in computational cost. In general, we find that the total energy of the LDA|CA|PAW and GGA|PW91|PAW methods decrease steadily from 300 eV to 500 eV with a gradient of -1×10^{-3} until convergence is effectively achieved at 500 eV with a spread thereafter of 1 and 5 meV, respectively.

In comparison to experiment the lattice constant prediction for the ZB structure, is given in table 2. The results show that the LDA|CA functional with the PAW basis set (LDA|CA|PAW) predicted lattice constants of ~5.30 Å over the range of plane-wave cut-offs, which is smaller than the average experimental value of 5.405 Å, although this underestimation is in line with other LDA calculations of ZnS, as referenced in table 2. In contrast, we find that the GGA calculations predicted lattice constant values in the range 5.437 – 5.450 Å which is closer to the reported experimental values and represents an overestimation ranging from 0.6-0.83%.

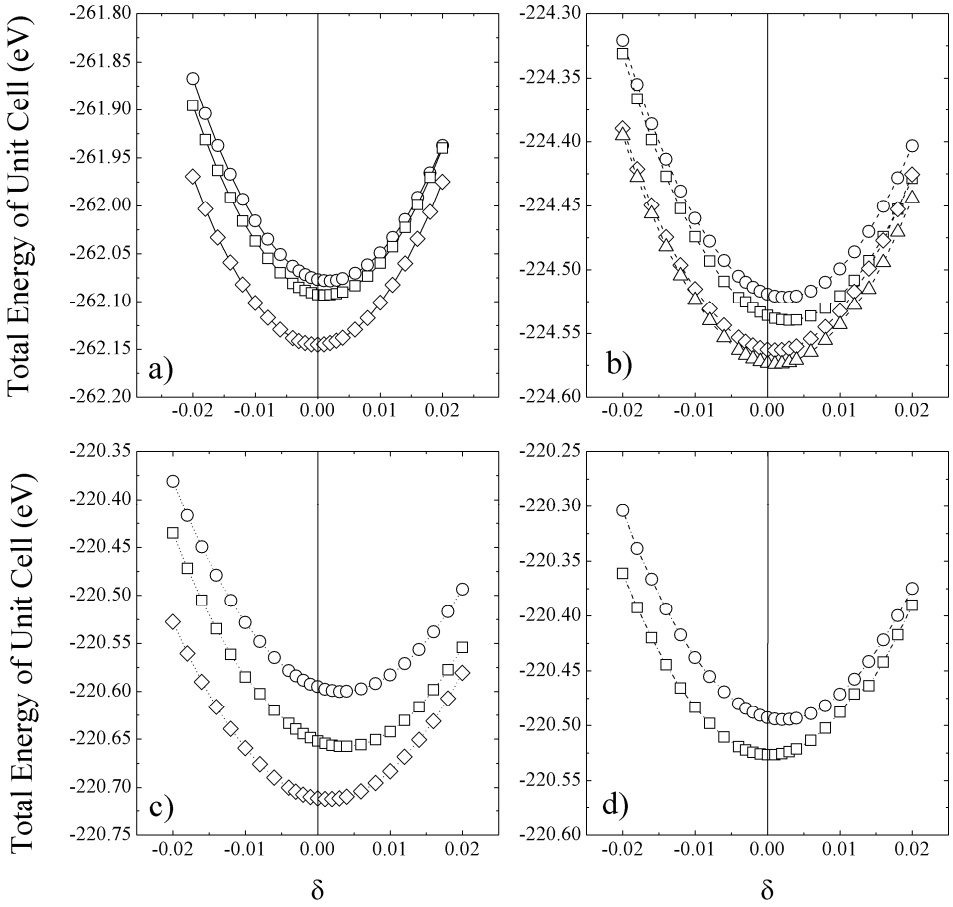

Fig. 4 Total cell energy as a function of elastic strain δ, used in determining the C_{11} elastic constant for the ZB structure. Calculated using **a)** LDA|CA|PAW with plane-wave cut-offs of 400(○), 425(□) and 500(◊) eV, **b)** GGA|PBE|PAW at 360(○), 420(□) 470(◊) and 500(**Δ**) eV, **c)** GGA|PW91|PAW at 360(○) 425(□) and 500(◊) eV and **d)** the GGA|PW91|USPP at 300(○) and 500(□) eV.

In regard to mechanical properties, figure 3 shows the variation of total lattice energy of the ZB phase with volume for all XC functional/basis set combinations. As expected, in each case the DFT lattice energy varies quadratically for small distortions about the equilibrium volume. Using the data shown in figure 3 the bulk modulus and pressure derivative of the bulk modulus were calculated for each functional-basis set combination using equation 1 and the results are shown in table 2 along with a list of other theoretical (DFT based) and experimental values.

From table 2 we observe that LDA|CA|PAW predicts the bulk modulus to be ~86 GPa with a variation of ~0.7% of this value when varying the plane-wave cut-off from 400 to 500 eV. The average of the published experimental ZnS (ZB) bulk modulus values (given in table 2) is 77.4 GPa, therefore LDA|CA|PAW overestimates the bulk modulus by ~10%.

The tendency for the LDA to underestimate the lattice constant and overestimate the bulk modulus is typical, as can be seen from previous LDA calculations referenced in table 2, and this suggests that for this material the LDA approximation overestimates the bond strength.

Alternatively, the overestimation of the lattice constant by GGA functionals is accompanied by an underestimation of the bulk modulus. GGA|PBE|PAW predicts the lattice constant of 5.443 to 5.449 over the plane-wave cut-off range of 360 to 500 eV, GGA|PW91|PAW predicts a slight smaller lattice constant, 5.437 to 5.443 over the same plane-wave cut-off range, and using ultrasoft pseudopotentials (GGA|PW91|USPP) also gave values close to those predicted by GGA|PBE|PAW and GGA|PW91|PAW. The predicted bulk modulus values for the GGA functionals range from 68.55 to 69.93 GPa across all pseudopotentials and basis set sizes, which is an underestimate of ~10% from the average of the experimental values, suggesting that the GGA approximation underestimates effective bond strength. It has been suggested previously that LDA calculations reproduce mechanical properties more accurately than GGA [13], however for ZnS (ZB) this is not the case.

The predicted values for the pressure derivative of the bulk modulus showed more variation but this is to be expected based on the functional form of equation 1. However most values for B_o' lie in the range 4 - 4.8 which is within the range of the experimentally reported values.

Figure 4 shows the parabolic fits of total energy *versus* the elastic strain δ used to calculate the C_{11} elastic constant for bulk ZnS (ZB). The predictions made within the GGA approximation are overall in very good agreement, although uniformly lower than the experimental value, laying within 10% of the experimental literature value 104.6 GPa. However it is interesting to note that for all the GGA functionals tested, the value of the C_{11} elastic constant decreased with increasing basis set size. The LDA|CA functional predicted higher values of ~117 GPa which is ~12.5% higher than the experimental value. As with the GGA functional's LDA|CA have a lower

Table 2 Summary of bulk constant calculations for the Zinc Blende (ZB) structure. The total memory required (Mem Req) refers to a single static point energy calculation of the fully relaxed structure (in gigabytes).

Method	a (Å)	B_o (GPa)	B'	C_{11} (GPa)	C_{12} (GPa)	E/N_{ZnS} (eV)	ΔH_f, S_8 (kJ/mol)	ΔH_f, S_2 (kJ/mol)	Mem Req (GB)
LDA|CA|PAW|400	5.300	86.179	4.517	117.485	70.526	-8.190	-176.22	-273.13	10.22
LDA|CA|PAW|425	5.302	86.541	3.954	117.175	71.223	-8.190	-176.51	-276.26	10.84
LDA|CA|PAW|500	5.304	85.897	4.632	116.331	70.680	-8.192	-176.56	-276.14	13.43
Other LDA	5.335[a]	83.7[a]	4.2[a]	123.7[a]	62.1[a]				
	5.328[b]	83.8[b]	4.5[b]	115.8[b]	72[b]				
	5.342[c]	89.67[c]	4.44[c]	118[c]	72[c]				
	5.339[d]	93.12[d]	4.63[d]						
	5.352[e]	83.1[e]	4.43[e]						
		82.0[f]	4.20[f]						
		84.2[g]	4.3[g]						
GGA|PBE|PAW|360	5.445	69.092	4.441	97.180	55.048	-7.013	-157.80	-238.69	9.16
GGA|PBE|PAW|420	5.443	69.030	4.527	96.649	55.220	-7.017	-157.66	-241.58	10.94
GGA|PBE|PAW|470	5.449	69.109	4.184	96.047	55.640	-7.018	-157.66	-241.59	13.09
GGA|PBE|PAW|500	5.448	68.550	4.520	94.780	55.435	-7.018	-157.88	-241.83	13.69
Other PBE	5.449[h]	70.020[h]	4.413[h]	97.206[h]	56.427[h]				
GGA|PW91|PAW|360	5.438	69.902	4.449	98.627	55.540	-6.894	-163.10	-246.99	9.04
GGA|PW91|PAW|425	5.437	69.876	4.404	97.786	55.922	-6.895	-162.86	-246.99	10.28
GGA|PW91|PAW|500	5.443	69.930	4.455	97.614	56.089	-6.897	-163.65	-247.82	13.37
Other GGA|PW91|PAW	5.60[i]	66.78[i]	3.95[i]						
GGA|PW91|USPP|300	5.446	69.591	5.481	95.052	56.860	-6.890	-167.87	-244.37	8.11
GGA|PW91|USPP|500	5.450	68.775	4.810	92.680	56.822	-6.891	-168.20	-247.40	13.97
Other GGA|PW91|USPP	5.404[j]	71.22[j]	4.705[j]	99.6[j]	57.0[j]				
Experimental	5.4102[l], 5.395[m], 5.410[m]	78.0[k], 74.8[l], 79.5[m]	4.91[l], 4[m]	104.6[k]	65.3[k]		-206.53[n] -105.4 [p] -30.25[q]		

[a] LDA FP-LMTO [14], [b] LDA Troullier-Martins [15], [c] LDA FP-APW+lo [16], [d] LDA LSDA FP-LAPW [17], [e] LDA PP-PW [18], [f] LDA LMTO [19], [g] LDA Troullier-Martins [20], [h] GGA PAW PBE [21], [i] GGA PAW PW91 [22], [j] GGA PAW PW91 [23], [k] Reference [24], [l] Reference [25], [m] Reference [26], [n] Reference [27], [p] Reference [28], [q] Reference [29].

C_{11} elastic constant with increasing basis set size, although this variation was less than 1% over the cut-off range of 400 to 500 eV.

Moving to the energetic properties, the predicted enthalpy of formation for ZnS (ZB), compared to the published experimental value, was uniformly high (~20% for GGA|PW91, ~24%for GGA|PBE and ~15% for LDA|CA) when using the S_2 molecule to estimate the chemical potential of sulphur (μ_S) and uniformly low (~20% for GGA|PW91, ~17%for GGA|PBE and ~34% for LDA|CA) when using the S_8 molecule as the basis for μ_S. However, it should be noted that the DFT predictions are calculated at zero temperature and pressure and the experimental value is determined at standard temperature and pressure (298 K, 1 atm). For all cases LDA|CA gave higher values for ΔH_f than GGA.

We believe these considerations would also apply to structures of lower dimensionality (for example slabs and rods), and summarises these tests in the following way:

- For bulk systems an 8 x 8 x 8 (Monkhorst-Pack) *k*-point mesh was adequate for sampling over the Brillouin zone. For structures of lower dimensionality, the same mesh density should be used in the periodic directions.
- A plane-wave cut-off of 500 eV is a safe value for calculating elastic moduli which require calculation of total energy with volumetric distortions, based on figure 2.
- For isotropic or symmetry preserving distortions (B_0 or $C_{11}+C_{12}$) an appropriate value for plane-wave cut-off can be lower than 500 eV.
- GGA gives more accurate predictions of cell parameters than LDA.
- LDA typically overestimates bond-strength in ZnS leading predictions of smaller cell parameters and larger values for elastic moduli compared to experiment.
- Conversely GGA underestimates bond-strength in ZnS leading to predictions of larger cell parameters and smaller values for elastic moduli compared to experiment.
- GGA shows remarkable uniformity in its predictions of structural (cell parameters), mechanical (elastic moduli) properties of ZnS with PBE and PW91 giving very similar results largely independent of basis set type (USPP or PAW) or basis set size (over the cut-off range considered).
- LDA predicts larger values for formation enthalpy over GGA and it is not possible to determine which of these gives results closer to experiment as this is also dependent on the appropriate choice of material for calculating the chemical potentials.

- In terms of formation enthalpy, the GGA|PBE|PAW results are converged for plane-wave cut-offs greater than 420 eV and GGA|PW91 results seem to converge at 500 eV independent of the basis set used.
- In terms of memory requirements for the calculation, the only consideration is plane-wave cut-off.

References

1 B. Gilbert, F. Huang, Z. Lin, C. Goodell, H. Z. Zhang, J. F. Banfield, *Nano Lett.* 2006, **6,** 605.
2 F. Huang, B. Gilbert, H. H. Zhang, J. F. Banfield, *Phys. Rev. Lett.* 2004, **92**, 4.
3 K. Murakoshi, H. Hosokawa, N. Tanaka, M. Saito, Y. Wada, T. Sakata, H. Mori, S. Yanagida, *Chem. Commun*. 1998, 321.
4 J. Nanda, S. Sapra, D. D. Sarma, N. Chandrasekharan, G. Hodes, *Chem. Mat.* 2000, **12** 1018.
5 S. B. Qadri, E. F. Skelton, A. D. Dinsmore, J. Z. Hu, W. J. Kim, C. Nelson, B. R. Ratna, *J. Appl. Phys*. 2001, **89** 115.
6 H. Tong, Y. J. Zhu, L. X. Yang, L. Li, L. Zhang, J. Chang, L. Q. An, S. W. Wang, *J. Phys. Chem. C* 2007, **111** 3893.
7 H. Z. Zhang, B. Gilbert, F. Huang, J. F. Banfield, *Nature,* 2003, **424** 1025.
8 J. P. Perdew, Y. Wang, *Phys. Rev. B* 1992, **45,** 13244.
9 J. P. Perdew, K. Burke, M. Ernzerhof, *Phys. Rev. Lett*. 1996, **77,** 3865.
10 D. M. Ceperley, B. J. Alder, *Phys. Rev. Lett*. 1980, **45** 566.
11 F. Benkabou, H. Aourag, M. Certier, *Mater. Chem. Phys.* 2000, **66**, 10.
12 J. C. Boettger, *Phys. Rev. B* 1997, **55**, 11202.
13 J. Hafner, *J. Comput. Chem.* 2008, **29**, 2044.
14 R. A. Casali, N. E. Christensen, *Solid State Comm*. 1998, **108**, 793.
15 S. Q. Wang, *J. Cryst. Growth* 2006, **287**, 185.
16 R. Khenata, A. Bouhemadou, M. Sahnoun, et al., *Comput. Mater. Sci.* 2006, **38**, 29.
17 M. Rabah, B. Abbar, Y. Al-Douri, et al., *Mater. Sci. Eng. B,* 2003, **100**, 163.
18 A. Qteish, A. Munoz, *Phys. Stat. Sol. B*, 2001, **223**, 417.
19 S. Ves, U. Schwarz, N. E. Christensen, et al., *Phys. Rev. B,* 1990, **42**, 9113.
20 J. Lopez-Solano, A. Mujica, P. Rodriguez-Hernandez, et al., *Phys. Stat. Sol. B*, 2003, **235**, 452.
21 M. Bilge, S. O. Kart, H. H. Kart, et al., *Mater. Chem. Phys*. 2008, **111**, 559.
22 F. A. Sahraoui, S. Zerroug, L. Louail, et al., *Mater. Lett.* 2007, **61**, 1978.
23 X. R. Chen, X. F. Li, L. C. Cai, et al., *Solid State Comm.* 2006, **139**, 246.
24 D. Berlincourt, H. Jaffe, and L. R. Shiozawa, *Phys. Rev.* 1963, **129**, 1009.
25 J. C. Jamieson and H. H. Demarest, *J. Phys. Chem. Solids* 1980, **41**, 963.
26 S. Desgreniers, L. Beaulieu, I. Lepage, *Phys. Rev. B*, 2000, **61**, 8726.
27 S. Deore, F. Xu, and A. Navrotsky, Am. Mineral. 2008, **93**, 779.
28 K. D. Daskalakis, G. R. Helz, Geochim. Cosmochim. Acta, 1993, **57**, 4923
29 K. Hayashi, A. Sugaki and A. Kitakaze, Geochim. Cosmochim. Acta, 1990, **54**, 715.